Faraday Discussions

Accepted Manuscript

This manuscript will be presented and discussed at a forthcoming Faraday Discussion meeting. All delegates can contribute to the discussion which will be included in the final volume.

Register now to attend! Full details of all upcoming meetings: http://rsc.li/fd-upcoming-meetings

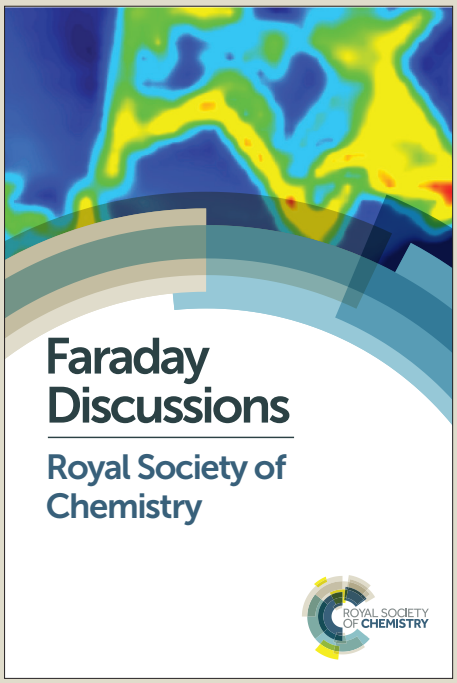

This is an *Accepted Manuscript*, which has been through the Royal Society of Chemistry peer review process and has been accepted for publication.

Accepted Manuscripts are published online shortly after acceptance, before technical editing, formatting and proof reading. Using this free service, authors can make their results available to the community, in citable form, before we publish the edited article. We will replace this *Accepted Manuscript* with the edited and formatted *Advance Article* as soon as it is available.

You can find more information about *Accepted Manuscripts* in the Information for Authors.

Please note that technical editing may introduce minor changes to the text and/or graphics, which may alter content. The journal's standard Terms & Conditions and the Ethical guidelines still apply. In no event shall the Royal Society of Chemistry be held responsible for any errors or omissions in this *Accepted Manuscript* or any consequences arising from the use of any information it contains.

ROYAL SOCIETY OF CHEMISTRY

www.rsc.org/faraday_d

Unfolding the contents of sub-nm plasmonic gaps using normalising plasmon resonance spectroscopy

Bart de Nijs,[a] Richard W. Bowman,[a] Lars O. Herrmann,[a] Felix Benz,[a] Steve J. Barrow,[b] Jan Mertens,[a] Daniel O. Sigle,[a] Anna Eiden,[c] Andrea Ferrari,[c] Oren A. Scherman,[b] Jeremy J. Baumberg*[a]

DOI: 10.1039/b000000x [DO NOT ALTER/DELETE THIS TEXT]

Plasmonic coupling of gold nanoparticles to a gold surface creates intense plasmonic hot spots with large electromagnetic field-enhancements within the cavity formed by the two metallic surfaces. The localised field in such structures is extremely sensitive to morphological fluctuations and subtle changes in the dielectric properties of the cavity contents. Here, we present an optical method that pins down the properties of the gap contents with high sensitivity, termed normalising plasmon resonance (NPR) spectroscopy. We use this on a variety of ultrathin molecular spacers such as filled and empty cucurbiturils, and graphene. Clear differences in the spectral positions and intensities of plasmonic modes observed in the scattering spectrum resolve thickness differences of 0.1nm, and refractive index changes from molecular filling.

[a] *NanoPhotonics Centre, Cavendish Laboratory, Department of Physics, JJ Thompson Ave, University of Cambridge, Cambridge, CB3 0HE, UK. Tel: 01223 760945; E-mail: jjb12@cam.ac.uk*
[b] *Department of Chemistry, University of Cambridge, Lensfield Road, Cambridge CB2 1EW, UK. Tel: 01223 331508; E-mail: oas23@cam.ac.uk*
[c] *Cambridge Graphene Centre, University of Cambridge, 9 JJ Thomson Avenue, Cambridge CB3 0FA, UK. Tel: 01223 748351; E-mail: acf26@cam.ac.uk*

Introduction

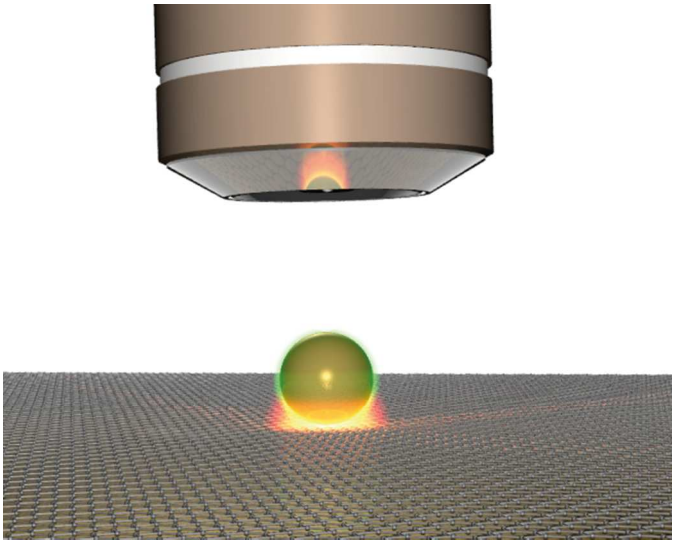

Figure 1: Depiction of a gold nanoparticle on a gold surface with a 0.34 nm thick graphene spacer. Locations of transverse mode (green) and coupled mode (red) shown schematically.

When metal nanostructures are brought into close proximity, their electromagnetic (EM) fields couple resulting in intensely localised plasmonic hot spots confined to the gap between the structures[1]. This plasmonic coupling can result in large field-enhancements[2] making these systems promising surface enhanced Raman scattering (SERS) substrates[3–5]. For example, when a gold nanoparticle (AuNP) is placed just above a gold surface, currents induced in the AuNP couple to the induced image charges in the gold surface forming a virtual dimer with a plasmonic hot spot centred in the cavity between the nanoparticle and the substrate[6–9]. This gold nanoparticle on mirror (NPoM) geometry has proved to be a powerful SERS substrate with enhancements allowing single molecule analysis[9,10].

In this geometry two distinct plasmonic resonance modes are typically identified. Firstly, the characteristic *transverse* plasmonic resonance mode (T) for gold nanoparticles (around 533 nm for 80 nm Au NPs) denotes charge oscillations parallel to the gold surface and is therefore essentially unaffected by the thickness or dielectric properties of the cavity. Secondly, the coupled mode (C) results from the interaction of the EM fields of the nanoparticle and surface giving a red-shifted resonance[11]. This second mode is tightly confined within the small cavity formed between the two metallic interfaces with a resonant wavelength that increases strongly with decreasing gap spacing. Especially for sub-nm gaps, angstrom sensitivities in the spacer thickness are reached[12–15]. In addition, the plasmonic mode in the gap is highly sensitive to the dielectric properties of the spacer material which allows us to develop a new type of 'normalised' plasmon resonance (NPR) spectroscopy. That this mode results from the coupling can be shown by using a non-metallic substrate such as glass on which no C-mode is observed, as shown in figure S1 in the supporting information.

Results

We show how it is possible to develop an optical analysis utilising the high sensitivity of the C mode in order to probe the properties of sub-nm gaps by collecting scattering spectra of individual nanoparticles. It provides the additional information by comparing mode intensities using the uncoupled T mode as a reference. We demonstrate this on a prototypical plasmonic system but it is widely applicable across many nanostructures and devices.

To study the effect of the spacer material in coupled plasmonic structures, 80 nm Au NPs are deposited on a gold coated silicon wafer supporting a thin spacer layer. Other NP sizes can be equally well used, but below 20nm diameter the spectral shifts can be too small for effective peak separation in the analysis below. Four different spacer layer systems are explored here: graphene (figure 1), monolayers of cucurbit[7]uril (CB[7], a rigid barrel shaped molecule), CB[7] with methyl viologen (MV^{2+}) as a guest, and CB[7] which is allowed to collect trace levels of molecules or ions from an aqueous solution over time.

In dark-field optical microscopy the 80 nm Au NPs on the gold surface in the NPoM geometry can be easily identified from their strong plasmonic scattering. A typical dark-field image shown in figure 2a resolves numerous Au NPs deposited on the gold surface with, in this case, CB[7] as a spacer layer with a spacing[3] of 0.9 nm. The two insets show two individual Au NPs, for which the dark field scattering spectra are presented in the subsequent figures 2b and c.

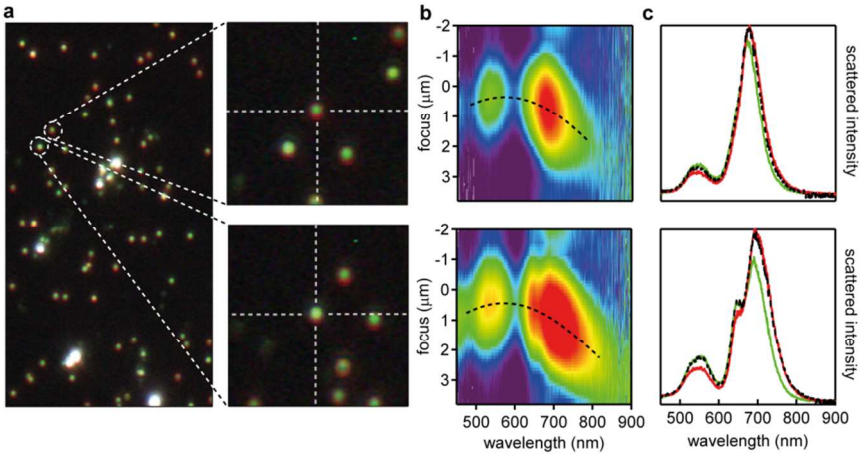

Figure 2: Dark field images and spectra showing the NPoM scattering properties of Au NPs on Au seperated by a 0.9 nm cucurbit[7]uril spacer. **a**) Dark field optical microscopy image showing scattering from many NPoMs, insets shows two typical nanoparticles with centre of collection spot indicated by white dashed lines. **b**) Focal-stack of scattering spectra from the two particles from (**a**) showing the effect of chromatic aberration. **c)** Scattering spectra at different focal heights, 0.35 µm (green) and 0.65 µm (red, top) or 1.05 µm (red, bottom), showing changes in peak ratios, with aberration corrected spectrum in black.

Spectral analysis when using microscopy objective lenses suffers from chromatic aberration, resulting in different focal points for each wavelength. In order to compare C mode intensities, the scattering spectra over a range of >5 µm focal distance are collected for each nanoparticle (figure 2b). This shows the strong effect of chromatic aberration for this lens (×100, NA0.8). Using Gaussian fits to the

depth-dependent scattering for each wavelength of the focal-stack allows us to extract the focal positions (black dashed line). Using the scattering intensity along the focal line, we thus correct for axial chromatic aberration, producing the spectra shown in black in figure 2c. These can be compared to spectral cuts at focal heights of 0.35 µm (green) and 0.65 µm (red, top) or 1.05 µm (red, bottom), which produce different ratios of the two plasmons' strengths. The green curve shows the scattering spectrum at a focal height optimising the T mode at 533 nm, whilst the red curve shows the spectrum at the optimal focal height for the C modes between 600 nm and 800 nm. Scanning through the focal range not only eliminates the effects of chromatic aberration but also makes the method insensitive to changes in focal height when comparing nanoparticles.

To analyse the properties of the different spacers, chromatic aberration corrected spectra of a large (up to 1600) set of nanoparticles are recorded for each sample. A computer controlled stage is automatically scanned around to locate and measure each nanoparticle-on-mirror in turn, with reproducibility in spectra better than 1%. A typical example of the resulting spectra is shown in figure 3a where 700 superimposed corrected scattering spectra are shown for 80 nm Au NPs on a gold surface with a spacer of empty CB[7]. The majority of these spectra show a transverse peak around 533 nm and T modes visible between 700-800nm.

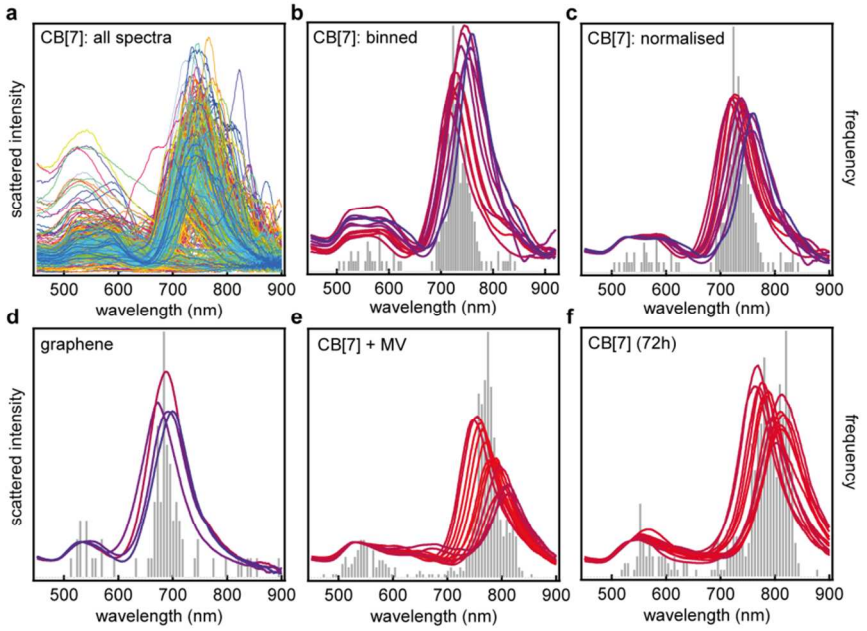

Figure 3: Scattering spectra of 80 nm Au NPs corrected for chromatic aberration with statistical peak distributions shown in grey. **a**) Superimposed spectra from 700 nanoparticles on Au with a CB[7] spacer showing two plasmon modes at 533 nm (T) and ~750 nm (C) (for the majority of the spectra). **b**) Spectra from (**a**) sorted into bins and averaged. Bins with <1% of the spectra are not shown. **c-f**) Spectra normalised to the maximum of the C mode at 533 are shown for spacers of **c**) CB[7], **d**) graphene, **e**) CB[7] sequestering methyl viologen (MV^{2+}) , and **f**) CB[7] left in solution for 72 h.

To determine the averaged intensity of the plasmonic peak for each wavelength the

spectral range from 450 nm to 900 nm is divided into 80 bins of 5.7 nm width, and the spectra sorted into these bins according to the position of the C mode. The resulting averaged spectra are shown in figure 3b together with the number of spectra found for each respective bin, shown in grey. Excluded from this analysis are spectra containing more than one coupled plasmon resonance peak, as previously reported for Au NPs on graphene[8], which are likely due to faceting of the AuNP as suggested by Sigle *et al.*[16] This minimizes the influence of more non-spherical nanoparticles in the analysis.

Averaging the resulting spectra from each bin results in sharp peaks for the C mode with nearly identical shapes. In addition, the distribution of bin frequencies of the individual spectral peaks is a narrow Gaussian (figure 3c-f in grey) which for CB[7] alone has a FWHM of 15 nm. An increase in the absolute intensity of both the T and C mode is observed as the position of the C mode moves towards the infrared. This is likely produced by the polydispersity of the Au NPs, with larger nanoparticles red-shifted and scattering more strongly. Normalising all spectra to their T mode intensity at 533 nm results in a set of near-identical peaks with (for CB[7] alone) comparable intensity ratios of 1:5 between the T and C mode (figure 3c). While a third plasmon mode of quadrupolar nature is visible at 600 nm, it does not affect the analysis.

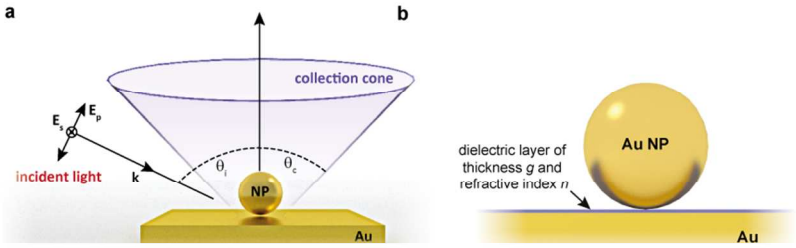

Figure 4: FDTD simulation geometry. **a**) Particle illuminated with *s*- and *p*-polarized plane waves at angle θ_i and scattered light collected over a cone with half-angle θ_c. This replicates the experimental dark-field geometry. **b**) Molecular or semiconductor monolayer in the gap modelled as an infinite dielectric sheet of thickness g (which determines the gap) and real refractive index n.

Using graphene as a spacer layer results in an even narrower FWHM of 13.4 nm with a distribution of coupled plasmon peak positions that is centred around 686 nm and with intensity ratio of 5.9 (figure 3d). This clearly demonstrates that changing the spacer layer strongly affects the characteristics of the C mode. Filling the CB[7] molecules with MV^{2+} prior to deposition on the gold surface results in a strong red shift of the C mode with a narrow FWHM of 14.5 nm. For this spacer the C peaks are centred around 773 nm and a decrease in the intensity ratio to between 4.5 to 3.2 is observed (figure 3e).

We find that leaving the empty CB[7] molecules bound to the gold surface in pure water over 3 days results in a significant cumulative shift in the coupled plasmon resonance peak. This is likely the result of CB[7] sequestering small molecules or ions from the water. This filling leads to two distinct populations in the distribution (figure 3f), where one group is spectrally located at 785 nm and the other at 805 nm. The two groups have intensity ratios of 5.3 and 4.5, respectively. We conclude that two or more types of molecules are sequestered in the CB[7] this way which results in the observation of two populations. This shows the extreme sensitivity of the

construct analysed in this way.

To better understand the coupled peak positions (λ_c) and intensity ratios (I_r), a series of numerical Finite-difference time-domain (FDTD) simulations are performed for the NPoM geometry. Here, the same collection cone of the objective (θ_c) and the same angle of incidence for *s*- and *p*-polarized light (θ_i) as in our experiments are used (figure 4a). The thickness of the spacer (g) is varied in the simulations between 0.5 nm to 3 nm and the refractive index (n) is changed from 1.2 to 1.8 (figure 4b). The resulting resonance map for thickness and refractive index is plotted in figure 5 (lines). This highlights how the measured λ_c and I_r can be conformally mapped into the cavity contents. Extreme care has to be taken to ensure both convergence of the simulations in such atomic-scale geometries, as well as appropriate modelling of the experimental conditions.

Plotting the intensity ratios versus the coupled plasmon peak positions for each of the different spacer layers in one graph shows a clear distinction between them all (figure 5). Pleasingly, comparing the experimental results with the simulations shows a good agreement with expected spacer thicknesses for CB[7] (0.9 nm) and graphene (0.4 nm). In addition, the results from the simulations suggest that the filling of CB[7] molecules with MV^{2+} results in a larger gap spacing, which is hard to infer from any other technique. This is indeed not surprising as the MV^{2+} molecular length is greater than the 0.9 nm height of the CB[7] molecules. This

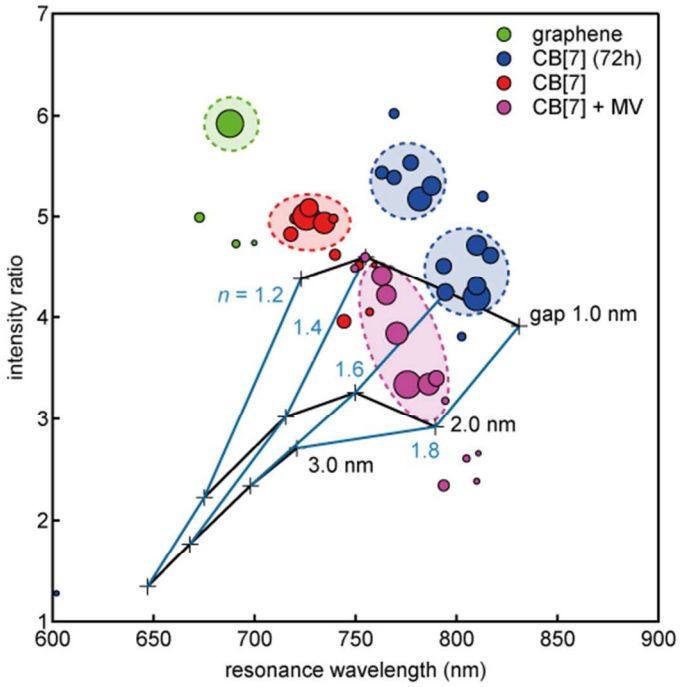

Figure 5: Intensity ratios for each of the different spacers plotted against the resonance wavelength over results obtained from simulations using different spacer thickness and refractive indices.

shows that 0.1 nm accuracy appears to be available from this NPR spectroscopy.

In addition, the filling of the CB[7] molecules with MV^{2+} is found to result in an

increase of the refractive index from <1.2 to between 1.4-1.7. By comparison, the resonance of initially empty NPoMs with CB[7] spacers that fill in solution over time shows a similarly strong increase in the refractive index from <1.2 to 1.4-1.6 with only a small variation in the gap spacing. This is likely due to mopping up of trace species in solution by the CBs, which can expel and replace the water molecules from inside, thus increasing the average electron density. Such changes have been noted from NMR studies on CBs[17], and are here found in real time optical spectroscopy on 10 nm^3 volumes.

This NPR technique thus has great utility in studying nanoscale and molecular structures and their chemical modifications, in ambient conditions and in real time. It thus opens up a wide range of applications for utilising nano-optics for nano-chemistry.

Conclusions

We present a spectral protocol and analysis method to study the properties of sub-nm gaps between Au NPs and Au surfaces. This requires correcting chromatic aberrations that are inevitably present in refractive lens based microscopy setups, but can be automated to deliver unbiased statistical samples. By comparing the intensities of the highly confined coupled plasmon with the unaffected transverse mode, a clear distinction between different sub-nm spacer layers is observed. Comparing the results from experiments with full simulations shows good agreement, recovering expected values for the different spacer layer thicknesses. This NPR spectroscopy reveals simple ways to monitor the contents of host-guest molecular systems, under real conditions. Our study thus opens up a new route for all-spectroscopic analysis of the thickness and refractive index of sub-nm cavities, thin films, molecular spacers and other ultrathin layers for controlled separation in plasmonics, electronics, and molecular nanodevices.

Methods

Substrate preparation:

For gold substrates, silicon wafers are coated using electron-beam-evaporation of a 70 nm thick gold layer on a 5 nm chrome adhesive layer. The surface roughness of the film is minimised by choosing a slow evaporation rate of 0.1 A/s. The gold coated substrate is submerged in a 1 mM solution of CB[7] in de-ionized water for 4 hours to deposit a layer of CB[7] molecules. For the MV^{2+} filled CB[7] sample a 1:1 molar ratio of CB[7] and MV is mixed and diluted to 1 mM and deposited on the gold surface as described for the empty CB[7] molecules. For the filling of the CB[7] molecules over time the gold substrate is submerged in a 1mM CB[7] solution and left for 72 h. The graphene samples were prepared by chemical vapour deposition (CVD) on a copper substrate and transferred onto the gold film using a standard PMMA transfer technique as described in more detail in reference [9].

Sample preparation:

The 80 nm citrate capped gold nanoparticles (Au NPs) from BBI are used as received. For all CB[7] samples, a 5 µL drop of 80 nm AuNP suspension is deposited on the coated film where physisorption takes place, and is rinsed off with

de-ionized water after 20 sec. (5 min. for graphene) to remove excess particles. The substrate is then blown dry using nitrogen. Using smaller Au NPs shifts the c-mode close to the t-mode and becomes weaker, as is shown in S2, using larger Au NPs shifts the c-mode further towards the infrared, therefore 80 nm Au NPs were used since they scatter more strongly compared to the 60 nm Au NPs but still have a resonance in, or near to, the visible range.

Spectral acquisition:

Spectra were collected using an Olympus BX51 optical microscope with an MPlanFLN 100x/ 0.80 dark-field objective fibre-coupled with a 50 µm VIS/NIR optical fibre to an Ocean Optics QE65pro spectrometer. To collect large data sets of AuNPoM scattering spectra, in-house particle tracking software was used. This software identifies particles based on a scattering intensity threshold and combined with a Prior Scientific *xyz*-motorized stage scans iteratively 9 spectral intensities in a 0.36 μm^2 map adjusting the *xy*-position accordingly to centre the collection spot on the AuNPoM. The final focus stack is then obtained by collecting 25 spectra over a focal range of 5.5 µm using a 1 second integration time.

Spectral analysis:

The spectra are isolated by fitting a multi Gaussian fit over the range between 500 nm and 900 nm. The spectra are sorted and averaged in bin sizes of 5.7 nm. If more than one peak is found between 600 nm and 900 nm with an amplitude of more than half of the C mode, the spectra is considered to have a double-peaked coupled plasmon mode and is sorted out thereby minimizing the influence of non-spherical nanoparticles in the analysis.

Simulations:

Numerical simulations are carried out using Lumerical FDTD Solutions v8.9. The AuNP was modelled as a sphere on top of an infinite dielectric sheet of thickness g. The sheet thickness was varied between 0.5 and 3.0 nm. Underneath this sheet, a 200 nm thick gold layer was placed in order to replicate the experimental NP on mirror geometry. The dielectric function of gold was taken from Johnson and Christy[18] and the real refractive index of the dielectric sheet was varied between 1.2 and 1.8. The NP was illuminated with an *s*- and *p*-polarized plane wave from an angle of incidence of θ_i=55°. The scattered light was then collected within a cone of half-angle θ_c=53° based on the numerical aperture of the objective. The resulting spectra were incoherently added in order to obtain the unpolarised scattering response that is measured experimentally.

Acknowledgements:

We acknowledges financial support from EPSRC grant EP/G060649/1, EP/I012060/1, ERC grant LINASS 320503. Richard Bowman acknowledges financial support from Queens' College. Felix Benz acknowledges support from the Winton Programme for the Physics of Sustainability.

References

1. Savage, K. J. et al. Revealing the quantum regime in tunnelling plasmonics. *Nature*, 2012, **491**, 574–577.
2. Zou, S. & Schatz, G. C. Silver nanoparticle array structures that produce giant enhancements in electromagnetic fields. *Chem. Phys. Lett.*, 2005, **403**, 62–67.
3. Taylor, R. W. et al. Precise Subnanometer Plasmonic Junctions for SERS within Gold Nanoparticle Assemblies Using Cucurbit[n]uril 'Glue'. *ACS Nano,* 2011, **5**, 3878–3887.
4. Taylor, R. W. et al. In Situ SERS Monitoring of Photochemistry within a Nanojunction Reactor. *Nano Lett*., 2013, **13**, 5985–5990.
5. Kneipp, K., Kneipp, H. & Kneipp, J. Surface-Enhanced Raman Scattering in Local Optical Fields of Silver and Gold NanoaggregatesFrom Single-Molecule Raman Spectroscopy to Ultrasensitive Probing in Live Cells. *Acc. Chem. Res.*, 2006, **39**, 443–450.
6. Aravind, P. K., Rendell, R. W. & Metiu, H. A new geometry for field enhancement in surface-enhanced spectroscopy. *Chem. Phys. Lett.*, 1982, **85**, 396–403.
7. Aravind, P. K. & Metiu, H. The effects of the interaction between resonances in the electromagnetic response of a sphere-plane structure; applications to surface enhanced spectroscopy. *Surf. Sci.*, 1983, **124**, 506–528.
8. Mertens, J. et al. Controlling Subnanometer Gaps in Plasmonic Dimers Using Graphene. *Nano Lett.*, 2013, **13**, 5033–5038.
9. Li, L., Hutter, T., Steiner, U. & Mahajan, S. Single molecule SERS and detection of biomolecules with a single gold nanoparticle on a mirror junction. *Analyst*, 2013, **138**, 4574–4578.
10. Taylor, R. W. et al. Watching individual molecules flex within lipid membranes using SERS. *Sci. Rep.*, 2014, **4**.
11. Mock, J. J. et al. Distance-Dependent Plasmon Resonant Coupling between a Gold Nanoparticle and Gold Film. *Nano Lett.*, 2008, **8**, 2245–2252.
12. Hao, E. & Schatz, G. C. Electromagnetic fields around silver nanoparticles and dimers. *J. Chem. Phys.*, 2004, **120**, 357–366.
13. Zuloaga, J., Prodan, E. & Nordlander, P. Quantum Description of the Plasmon Resonances of a Nanoparticle Dimer. *Nano Lett.,* 2009, **9**, 887–891.
14. Marinica, D. C., Kazansky, A. K., Nordlander, P., Aizpurua, J. & Borisov, A. G. Quantum Plasmonics: Nonlinear Effects in the Field Enhancement of a Plasmonic Nanoparticle Dimer. *Nano Lett.*, 2012, **12**, 1333–1339.
15. García de Abajo, F. J. Nonlocal Effects in the Plasmons of Strongly Interacting Nanoparticles, Dimers, and Waveguides. *J. Phys. Chem. C*, 2008, **112**, 17983–17987.
16. Sigle, D. O. et al. Monitoring morphological changes in 2D monolayer semiconductors using atom-thick plasmonic nanocavities. *Submitted* 2014.
17. Kellersberger, K. A., Anderson, J. D., Ward, S. M., Krakowiak, K. E. & Dearden, D. V. Encapsulation of N 2 , O 2 , Methanol, or Acetonitrile by Decamethylcucurbit[5]uril(NH 4 +) 2 Complexes in the Gas Phase: Influence of the Guest on 'Lid' Tightness. *J. Am. Chem. Soc.*, 2001, **123**, 11316–11317.
18. Johnson, P. B. & Christy, R. W. Optical Constants of the Noble Metals. *Phys*. *Rev*. *B*, 1972, **6**, 4370–4379.